Methane airborne measurements and comparison to global models during BARCA

Beck, Veronika; Chen, Huilin; Gerbig, Christoph; Bergamaschi, Peter; Bruhwiler, Lori; Houweling, Sander; Rockmann, Thomas; Kolle, Olaf; Steinbach, Julia; Koch, Thomas

Published in:
Journal of geophysical research-Atmospheres

DOI:
10.1029/2011JD017345

Publication date:
2012

Methane airborne measurements and comparison to global models during BARCA

Veronika Beck,[1] Huilin Chen,[1,2] Christoph Gerbig,[1] Peter Bergamaschi,[3] Lori Bruhwiler,[4] Sander Houweling,[5,6] Thomas Röckmann,[5] Olaf Kolle,[1] Julia Steinbach,[1,7] Thomas Koch,[1] Célia J. Sapart,[5] Carina van der Veen,[5] Christian Frankenberg,[6,8] Meinrat O. Andreae,[9] Paulo Artaxo,[10] Karla M. Longo,[11] and Steven C. Wofsy[12]

Received 19 December 2011; revised 15 June 2012; accepted 28 June 2012; published 14 August 2012.

[1] Tropical regions, especially the Amazon region, account for large emissions of methane (CH_4). Here, we present CH_4 observations from two airborne campaigns conducted within the BARCA (Balanço Atmosférico Regional de Carbono na Amazônia) project in the Amazon basin in November 2008 (end of the dry season) and May 2009 (end of the wet season). We performed continuous measurements of CH_4 onboard an aircraft for the first time in the Amazon region, covering the whole Amazon basin with over 150 vertical profiles between altitudes of 500 m and 4000 m. The observations support the finding of previous ground-based, airborne, and satellite measurements that the Amazon basin is a large source of atmospheric CH_4. Isotope analysis verified that the majority of emissions can be attributed to CH_4 emissions from wetlands, while urban CH_4 emissions could be also traced back to biogenic origin. A comparison of five TM5 based global CH_4 inversions with the observations clearly indicates that the inversions using SCIAMACHY observations represent the BARCA observations best. The calculated CH_4 flux estimate obtained from the mismatch between observations and TM5-modeled CH_4 fields ranges from 36 to 43 mg m^{-2} d^{-1} for the Amazon lowland region.

Citation: Beck, V., et al. (2012), Methane airborne measurements and comparison to global models during BARCA, *J. Geophys. Res.*, *117*, D15310, doi:10.1029/2011JD017345.

1. Introduction

[2] Atmospheric methane (CH_4) has received much attention as the second most important greenhouse gas after carbon dioxide (CO_2). It has a global warming potential that is 25 times higher than that of CO_2 on a 100 year time horizon [*Intergovernmental Panel on Climate Change*, 2007]. About 30% of the CH_4 sources are thought to be of natural origin, of which almost 70% are emissions from anaerobic microbial production in wetlands [*Wuebbles and Hayhoe*, 2002]. Tropical regions account for 60% of the global wetland emissions [*Bartlett and Harriss*, 1993]. Therefore, the Amazon basin with its estimated CH_4 wetland emissions of 29.3 Tg a^{-1} is a strong natural source of CH_4 [*Melack et al.*, 2004]. Anthropogenic sources such as biomass burning and fossil fuel emissions also contribute significantly to the CH_4 emissions in the Amazon region [*Bousquet et al.*, 2006]. Aerobic CH_4 emissions by plants as first identified by *Keppler et al.* [2006] have been under controversial discussion as an additional source of atmospheric CH_4 for several years (see *Bergamaschi et al.* [2009] for a summary of the discussion), but have been found to be a rather small source [*Nisbet et al.*, 2009], and have not been identified in the field so far [*Querino et al.*, 2011].

[3] Several studies using CH_4 flux measurements have been carried out since the 1980s to quantify both, the natural wetland source and other natural sources of CH_4 such as emissions from soil or bromeliads [*Bartlett et al.*, 1990; *Crill et al.*, 1988; *Devol et al.*, 1988; *Carmo et al.*, 2006; *Martinson et al.*, 2010]. The contribution to the atmosphere from biomass burning was investigated by several aircraft

[1]Max Planck Institute for Biogeochemistry, Jena, Germany.
[2]Now at National Oceanic and Atmospheric Administration, Boulder, Colorado, USA.
[3]Institute for Environment and Sustainability, Joint Research Centre, European Commission, Ispra, Italy.
[4]Climate Monitoring and Diagnostics Laboratory, National Oceanic and Atmospheric Administration, Boulder, Colorado, USA.
[5]Institute for Marine and Atmospheric Research Utrecht, Utrecht University, Utrecht, Netherlands.
[6]SRON Netherlands Institute for Space Research, Utrecht, Netherlands.
[7]Now at Department of Applied Environmental Science, Stockholm University, Stockholm, Sweden.
[8]Now at Jet Propulsion Laboratory, California Institute of Technology, Pasadena, California, USA.
[9]Biochemistry Department, Max Planck Institute for Chemistry, Mainz, Germany.
[10]Applied Physics Department, University São Paulo, São Paulo, Brazil.
[11]Center for Earth System Science, National Institute for Space Research, São José dos Campos, Brazil.
[12]Department of Earth and Planetary Sciences, Harvard University, Cambridge, Massachusetts, USA.

Corresponding author: V. Beck, Max Planck Institute for Biogeochemistry, Hans-Knöll-Str. 10, DE-07745 Jena, Germany. (vbeck@bgc-jena.mpg.de)

0148-0227/12/2011JD017345

campaigns over the Amazon basin where flasks were taken during flights and analyzed for CH_4 [e.g., *Ferek et al.*, 1998; *Yokelson et al.*, 2007]. The main focus of these aircraft campaigns was to investigate the distribution of carbon monoxide (CO), ozone (O_3), and aerosols from biomass burning in the atmosphere over the Amazon basin [*Andreae and Merlet*, 2001; *Guyon et al.*, 2005]. Additionally, an aircraft campaign for estimating the carbon balance of the central Amazon took place in 2001 [*Lloyd et al.*, 2007]. From 2000 to the present, the National Oceanic and Atmospheric Administration Earth System Research Laboratory (NOAA-ESRL) has collected flask air samples of stationary vertical profiles over Manaus and Santarém on a regular basis [*Miller et al.*, 2007]. In addition to ground based and airborne measurements, total column measurements of CH_4 from space are available since 2003 using the SCanning Imaging Absorption spectroMeter for Atmospheric ChartograpHY (SCIAMACHY) satellite onboard ENVISAT [*Frankenberg et al.*, 2005, 2008, 2011], which has enabled global scale inverse modeling studies with strongly improved data coverage in the tropics. Still, there are large uncertainties on the CH_4 source strength particularly in the tropics [*Meirink et al.*, 2008a; *Bergamaschi et al.*, 2009].

[4] The BARCA project is part of the Large-scale Biosphere-Atmosphere (LBA) project [*Keller et al.*, 2009]. The main goal of the BARCA project is to quantify the greenhouse gas budgets for the Amazon basin by combining a top-down approach using aircraft observations and a bottom-up approach using observations from flux towers and process-based land surface models. Up to now, CH_4 (and also CO_2) atmospheric observations in the Amazon region are in most instances only available on a local scale (flux towers, stationary airborne profiles). Satellite observations (e.g., from the SCIAMACHY satellite) have quasi global coverage, but only limited accuracy. For a full understanding of the ongoing processes in the Amazon region and for the determination of the location of sources and sinks of greenhouse gases, data collection on the regional scale is essential. Therefore, regional-scale airborne measurements of greenhouse gases, aerosols, and ozone covering nearly the entire Amazon basin were accomplished within the BARCA project during two aircraft campaigns. Vertical cross-sections of the planetary boundary layer and lower free troposphere were flown in order to observe three-dimensional tracer distributions at high resolution.

[5] An extensive set of CH_4 data has been collected during the two BARCA campaigns. For the first time in the Amazon basin, continuous measurements of CH_4 onboard an aircraft were conducted using an analyzer based on the cavity ring-down spectroscopy (CRDS) technique (second campaign only). Additionally, flask samples were taken and analyzed for CH_4 during both campaigns. The continuous measurements provided the opportunity to capture a better picture of the distribution of CH_4 in the planetary boundary layer and lower free troposphere in the Amazon basin. Analysis of $\delta^{13}C$ and δD isotopes and CO mixing ratios as additional tracers enabled us to attribute observed CH_4 mixing ratios to different CH_4 source processes.

[6] By a comparison of the BARCA CH_4 observations with global model results constrained by observations from NOAA-ESRL surface stations and the SCIAMACHY satellite, we evaluate the performance of these models in the tropical regions, especially over the Amazon basin. Five different CH_4 inversions all based on the TM5 model [*Krol et al.*, 2005], with two of them using additional observational constraints from the SCIAMACHY satellite, are compared to BARCA CH_4 observations for November 2008 and May 2009 in five different sampling regions of the Amazon basin. The monthly budgets of the influence regions, which were derived from a Lagrangian Particle Dispersion Model (LPDM), of these five sampling regions are evaluated against the mismatch of modeled and observed CH_4 mixing ratios. From this evaluation, flux estimates for the Amazon lowland region are obtained that correct for the model-data mismatch.

[7] The paper is organized as follows: Section 2 describes the collection of the data, while section 3 deals with the analysis of the CH_4 observations. In section 4, the comparison between global CH_4 inversions and the BARCA observations is discussed. Finally, section 5 concludes the paper.

2. Data Collection During Two BARCA Campaigns

[8] We conducted two airborne measurement campaigns within the BARCA project using the Bandeirante research aircraft from the National Institute for Space Research (INPE)—one at the end of the dry season in November 2008 (BARCA-A) and the other at the end of the wet season in May 2009 (BARCA-B). The aim of these two measurement campaigns was to obtain a set of greenhouse gas and aerosol measurements across the whole Amazon basin by flying cross-sections through the planetary boundary layer and lower free troposphere between altitudes of 500 m and 4000 m. In total, data from over 150 vertical profiles were collected on 27 flights, nearly covering the full Amazon basin (Figure 1), during both campaigns. Table 1 shows an overview over all flights.

[9] A total of 174 and 206 flask samples were collected during BARCA-A and BARCA-B, respectively, which were subsequently analyzed for a set of various trace gases in the Jena Gaslab (including CH_4, CO, and sulfur hexafluoride, SF_6) and for $^{13}CO_2$ in the Jena Isolab. For CH_4 analysis, the NOAA04 scale was applied [*Dlugokencky et al.*, 2005]. Selected flask samples from both campaigns were sent to the Institute for Marine and Atmospheric Research Utrecht for CH_4 isotope analysis using an analytical system described in *Brass and Röckmann* [2010]. Isotope ratios are reported in the conventional δ notation as $\delta^{13}C = [{}^{13}R_{SA}/{}^{13}R_{ST} - 1]$ and $\delta D = [{}^{2}R_{SA}/{}^{2}R_{ST} - 1]$ where ${}^{13}R_i$ and ${}^{2}R_i$ are the ${}^{13}C/{}^{12}C$ and D/H ratios of a sample (i = SA) and an international Standard (i = ST), respectively. The international standards are Vienna PeeDeeBelemnite for $\delta^{13}C$ measurements and Vienna Standard Mean Ocean Water for δD measurements.

[10] During the second campaign (BARCA-B), a CRDS analyzer (Model G1301-m, Picarro Inc., CA, USA) was deployed onboard the aircraft for continuous measurements of CH_4, CO_2, and H_2O [*Chen et al.*, 2010] in addition to flask sampling. The CRDS analyzer reported the mixing ratios of CH_4 at time intervals of 3 s with a precision better than 1 ppb [*Chen et al.*, 2010]. Comparisons of continuous measurements against flask analysis results indicate that the accuracy of CH_4 measurements by the CRDS analyzer is better than 2 ppb [*Chen*, 2010].

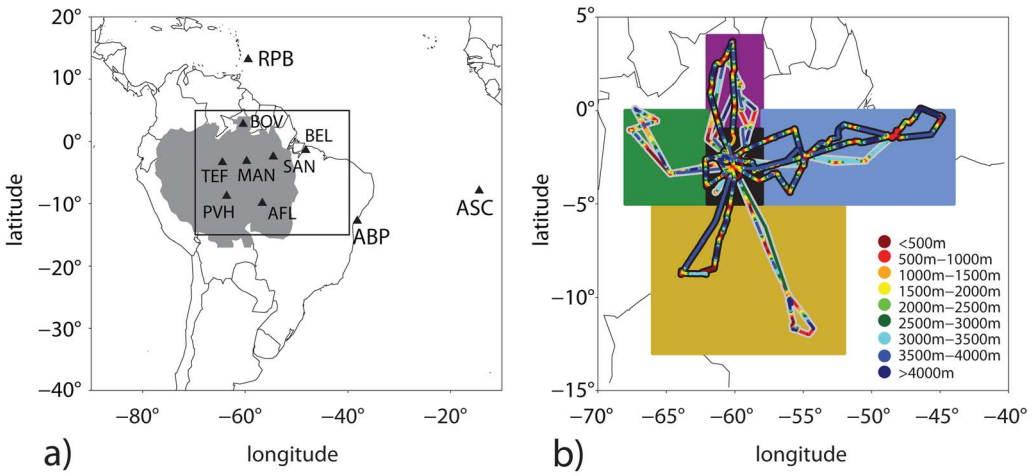

Figure 1. (a) Location of the NOAA-ESRL background stations Ragged Point Barbados (RPB), Ascension Island (ASC), and Arembepe (ABP) and the main cities in the Amazon basin: Manaus (MAN), Santarém (SAN), Belém (BEL), Boa Vista (BOV), Tefé (TEF), Porto Velho (PVH), and Alta Floresta (AFL). The gray shaded area depicts the Amazon lowland region (<500 m) as described in *Melack et al.* [2004]. (b) Illustrates the zoom into the black rectangular in Figure 1a and shows the flight tracks of BARCA-A (gray-shaded) and BARCA-B (black-shaded). Altitudes are denoted by different colors. The solid boxes illustrate the separation of the BARCA observations into five different sampling regions of the Amazon basin: north (violet), latitude >−1.0° and longitude >−62.0°; west (green), latitude >−5.0° and longitude <−62.0°; central (black), latitude >−5.0° and latitude <−1.0° and longitude >−62.0° and longitude <−58.0°; east (blue), latitude >−5.0° and latitude <0.0° and longitude >−58.0°; south (yellow), latitude <−5.0° (cf. Figures 3 and 7).

[11] Carbon monoxide (CO) was measured at 2-s time resolution by UV resonance fluorescence, using a Fast-CO-Monitor (Model AL 5002, Aerolaser GmbH, Germany). Prior to measurement, the air was dried using a Nafion drier. The precision of the 0.5 Hz data was 0.6%, based on the variability of the measurements of the standard gas within each 30-s calibration period. In flight, zero and span calibrations were made every 10 min to account for instrumental

Table 1. Overview Over All Flights Conducted During BARCA-A and BARCA-B Indicated With Their Flight Number, the Date of Each Flight, the Flight Origin and Destination, the Number of Vertical Profiles Flown, and the Number of Flasks Sampled

	Flight Number	Date	Direction	Number of Profiles	Number of Flasks
BARCA A	2	20081116	around Manaus	4	-
	3	20081118	Manaus-Santarém	4	13
	4	20081118	Santarém-Belém	4	17
	5	20081119	Belém-Santarém	6	17
	6	20081119	Santarém-Manaus	4	12
	7	20081122	around Manaus (north)	8	26
	8	20081123	Manaus–Boa Vista	8	14
	9	20081123	Boa Vista–Manaus	4	14
	10	20081125	Manaus–Alta Floresta	6	15
	11	20081126	around Alta Floresta	8	14
	12	20081127	Alta Floresta–Manaus	2	3
	13	20081129	Manaus–Tefé	4	12
	14	20081130	around Tefé (northwest)	8	17
BARCA B	2	20090517	around Manaus (west)	6	14
	3	20090517	around Manaus (west)	10	16
	4	20090519	Manaus–Boa Vista	10	18
	5	20090519	Boa Vista–Manaus	6	12
	6	20090521	Manaus-Santarém	8	14
	7	20090521	Santarém-Belém	6	16
	8	20090522	Belém offshore	4	15
	9	20090523	Belém-Santarém	6	13
	10	20090523	Santarém-Manaus	2	9
	11	20090526	Manaus-Santarém	8	14
	12	20090526	Santarém-Manaus	8	15
	13	20090527	Manaus–Porto Velho	8	13
	14	20090527	Porto Velho–Manaus	2	10
	15	20090528	around Manaus (city)	2	13

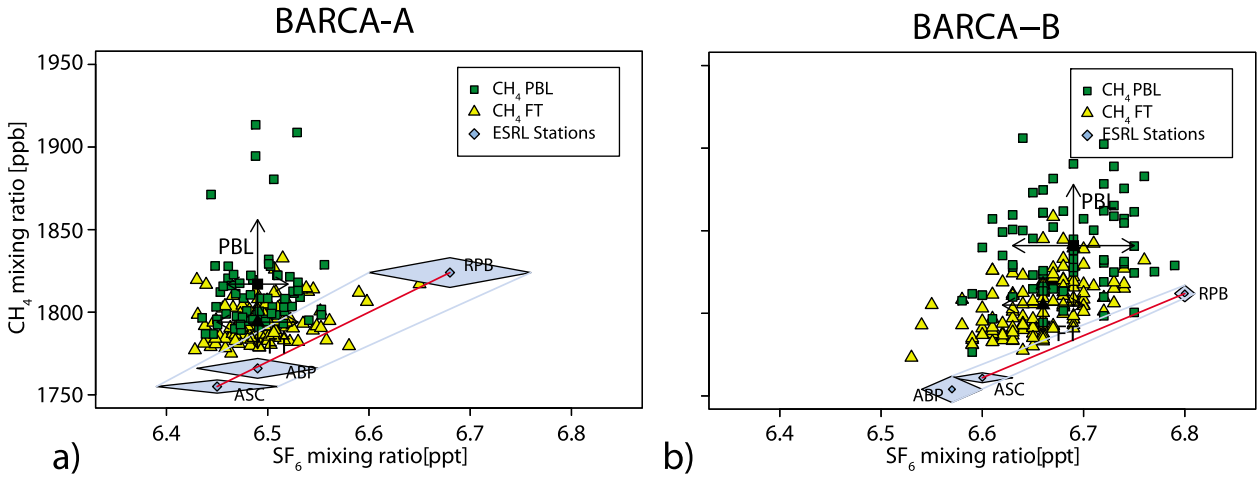

Figure 2. Methane mixing ratios as a function of SF_6 mixing ratios for all flasks collected during (a) BARCA-A and (b) BARCA-B. The CH_4 and SF_6 mixing ratios from the NOAA-ESRL surface stations (CH_4 and SF_6 data courtesy of E. Dlugokencky, NOAA-ESRL Global Monitoring Division GMD) at Ragged Point Barbados (RPB) representing northern hemispheric air, Ascension Island (ASC) representing southern hemispheric air, and Arembepe (ABP) at the Brazilian coast during the duration of the two campaigns are also shown. The red lines indicate the mixing line between northern and southern hemispheric air. The black squares illustrate the mean values of CH_4 and SF_6 for the planetary boundary layer (PBL; altitude <1250 m) and the free troposphere (FT; altitude >1250 m). The black error bars and the blue regions and lines show the 1-sigma standard deviation. In both panels, the flask sample with the highest observed CH_4 mixing ratio is not denoted (BARCA-A: 2050 ppb, BARCA-B: 2055 ppb).

drift associated with varying pressure and temperature. Further details can be found in the paper by *Andreae et al.* [2012].

3. Methane Data Analysis

[12] The measured CH_4 mixing ratios obtained during both BARCA campaigns are discussed in relation to the CH_4 mixing ratios observed at NOAA background stations east and northeast of the South-American continent within the same time period [*Dlugokencky et al.*, 2010]. Additionally, seasonal differences between the two campaigns that took place at the end of the dry season (BARCA-A) and at the end of the wet season (BARCA-B) are examined. In a second step, we use CO as an additional tracer and the isotopic composition of CH_4 to distinguish between different sources of CH_4, such as CH_4 emissions from anaerobic microbial production in wetlands, biomass burning, and other anthropogenic sources.

3.1. BARCA-A Versus BARCA-B

[13] To derive an estimate of the magnitude of CH_4 emitted from the Amazon basin, the CH_4 results from flask samples for BARCA-A and BARCA-B are compared to NOAA-ESRL measurements at the background stations Ascension Island (ASC, 7.92°S, 14.42°W) representing Southern hemisphere air, Ragged Point Barbados (RPB, 13.17°N, 59.43°W) representing Northern hemisphere air, and Arembepe (ABP, 12.77°S, 38.17°W) at the Brazilian coast. Flasks sampled at the three background stations during the time periods of the two BARCA campaigns are utilized for the comparison. Depending on the station, 4 to 12 flask samples are used. Note that the NOAA flasks are usually sampled for baseline conditions, i.e., in case of ABP only for onshore winds. To assess the role of interhemispheric mixing, CH_4 mixing ratios are plotted as a function of sulfur hexafluoride (SF_6) mixing ratios (Figures 2a and 2b) [cf. *Miller et al.*, 2007]. SF_6 is a purely anthropogenic gas, and serves as an excellent hemispheric tracer since almost all SF_6 is emitted in the Northern hemisphere [*Olivier et al.*, 1999]. Therefore, mixing of Northern hemispheric air, with high CH_4 mixing ratios, into the Southern hemisphere should proceed along the mixing lines between the two end-members in the CH_4-SF_6 space, as indicated in Figure 2. It is clear at first sight that almost all flask results show CH_4 values higher than this mixing line, which clearly indicates a CH_4 source in the Amazon basin.

[14] The measured CH_4 mixing ratios are separated into those sampled in the planetary boundary layer (altitudes <1250 m) and in the lower free troposphere (altitudes 1250–4500 m). For BARCA-A (Figure 2a), the mean SF_6 mixing ratio was 6.49 ± 0.03 ppt (1-sigma standard deviation) for the planetary boundary layer and 6.49 ± 0.04 ppt for the free troposphere. This clearly indicates that most of the background air sampled in the Amazon in November 2008 comes from the Southern hemisphere (ASC: 6.45 ± 0.06 ppt), while only a few flasks sampled in the free troposphere have SF_6 mixing ratios closer to the SF_6 mixing ratio measured at RPB (6.68 ± 0.08 ppt). The flasks with the highest SF_6 mixing ratios show CH_4 mixing ratios that follow the expected mixing line. On average, the value of the CH_4 mixing ratio during BARCA-A is 1817 ± 39 ppb in the planetary boundary layer and 1794 ± 12 ppb in the free troposphere which indicates an enhancement of ∼45 ppb and ∼25 ppb, respectively, compared to the mixing line between the NOAA-ESRL surface stations ASC (1755 ± 4 ppb) and RPB (1824 ± 9 ppb).

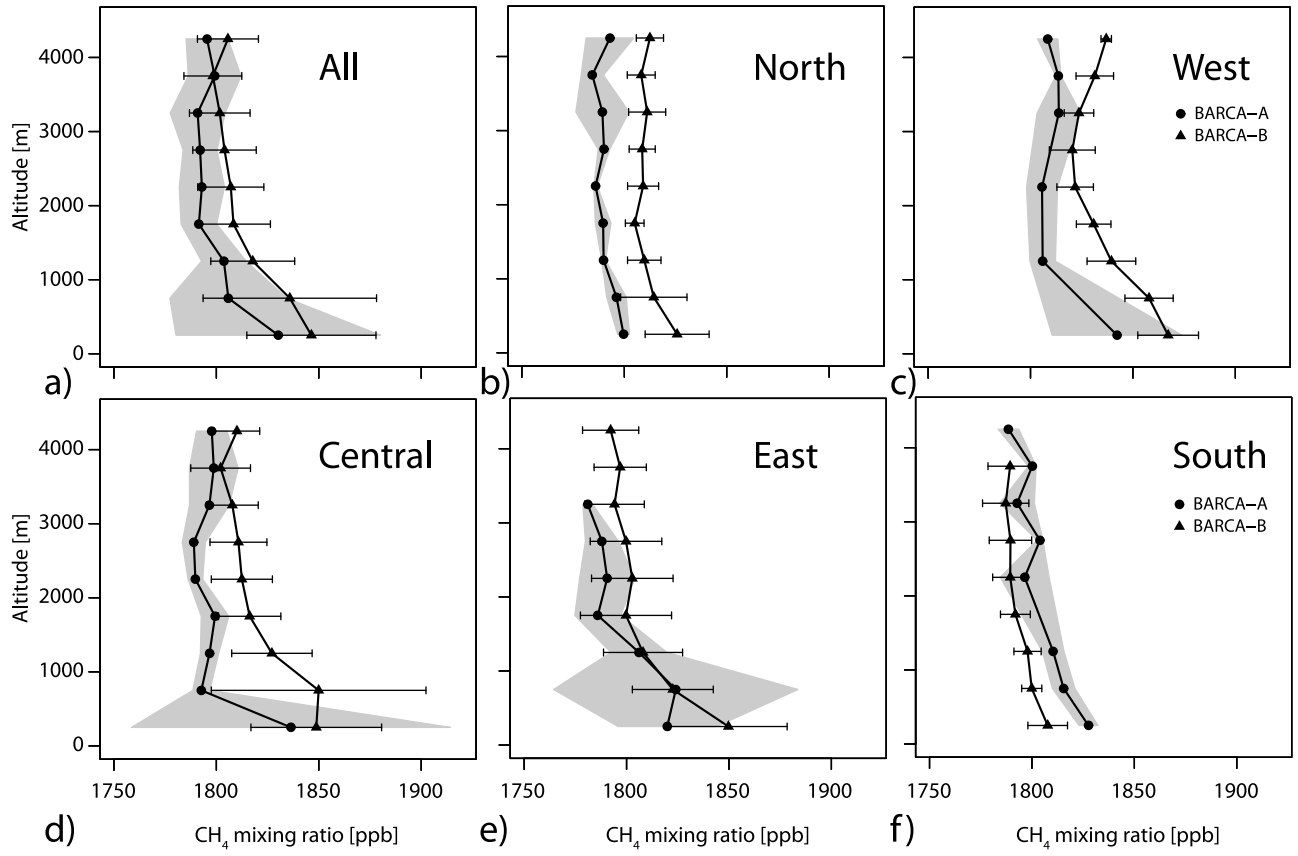

Figure 3. Five-hundred-meter binned vertical profiles for the observed CH_4 mixing ratios for (a) the total campaign average and (b–f) different regions of the Amazon basin. The mean vertical profiles are shown for BARCA-A and BARCA-B. The 1-sigma standard deviation of the observations is denoted as gray shaded area for BARCA-A and as error bars for BARCA-B. The Amazon basin is divided into northern, western, central, eastern and southern parts, as shown in Figure 1b.

[15] In contrast, for BARCA-B the airflow into the Amazon basin was a mixture of both hemispheres, as the measured SF_6 mixing ratios cover the entire range between the two end-members (Figure 2b). Similar to BARCA-A, the mean CH_4 mixing ratio observed in the planetary boundary layer (1841 $\pm$ 37ppb) and the free troposphere (1806 $\pm$ 38ppb) are enhanced $\sim$60 ppb and $\sim$25 ppb, respectively, compared to the mixing line between the background stations ASC (1761 $\pm$ 3 ppb) and RPB (1812 $\pm$ 5 ppb). During BARCA-B, continuous measurements using the CRDS analyzer are also available, and they show similar mean values as the flask measurements (1839 $\pm$ 37 ppb for the planetary boundary layer and 1805 $\pm$ 17 ppb for the free troposphere). This indicates clearly that the flask results are representative for large parts of the Amazon basin. We conclude from the observations that the Amazon basin is a strong source of CH_4 during both seasons.

[16] For a comparison of the vertical structure of atmospheric CH_4 between BARCA-A and BARCA-B in different regions of the Amazon basin (north, west, east, south and central—for definitions of the single regions, see Figure 1b), vertical profiles of the CH_4 mixing ratios were binned into 500-m intervals. Flask measurements were used to calculate the vertical profiles for BARCA-A, while for BARCA-B the continuous data from the CRDS analyzer were aggregated into 500-m binned profiles except for flights 8–10 (Table 1), where no continuous data were available due to instrument failure. For these flights, flask data were taken to calculate the profiles.

[17] As already illustrated in Figure 2, the mean values of CH_4 in the planetary boundary layer are on average 23 ppb lower for BARCA-A (1817 ppb) than for BARCA-B (1839 ppb). The difference between the mean CH_4 mixing ratios in the lower free troposphere during BARCA-A (1794 ppb) and BARCA-B (1806 ppb) is smaller (12 ppb) than for the planetary boundary layer. This is also seen in the total campaign averaged vertical profile and the vertical profiles for the different regions for BARCA-A and BARCA-B (Figure 3a). The mean vertical profiles for the different regions (Figures 3b–3f) denote an increase in the CH_4 mixing ratio at altitudes between 500 m and 1000 m during BARCA-B, especially for the western and the central part, while in the southern and eastern part during BARCA-A the mixing ratio at 500–1000 m was higher or equal compared to BARCA-B. The increase in the CH_4 mixing ratio in the southern part during BARCA-A may be explained by intensive biomass burning activity along the southern and eastern margins of the Amazon Basin in November 2008 compared to May 2009. This was demonstrated for CO and aerosol particle number concentrations by *Andreae et al.* [2012], where maps of the distributions of fires during the BARCA campaigns are shown. Noticeable is the higher

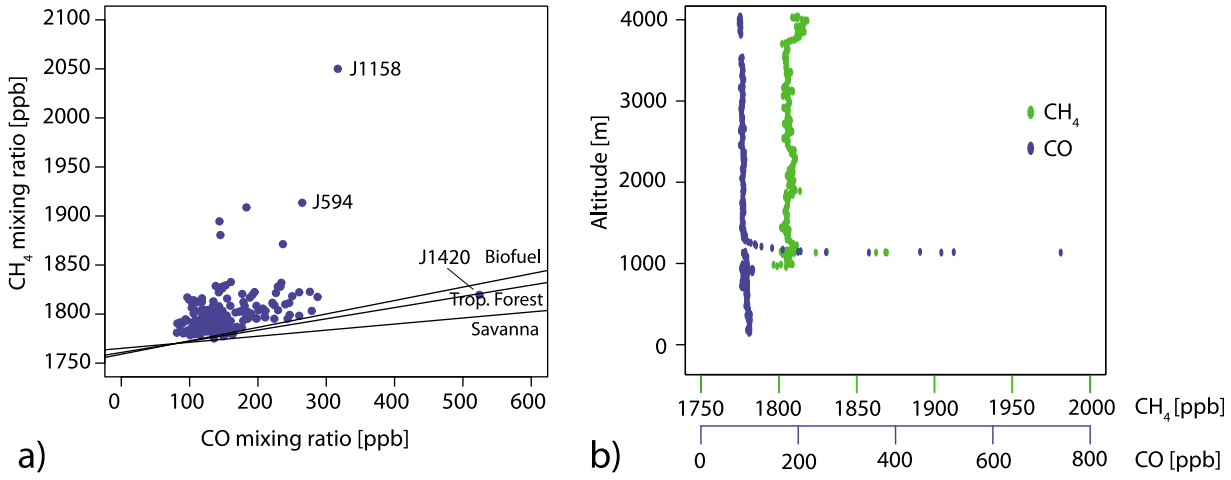

Figure 4. (a) Methane mixing ratio as a function of the CO mixing ratio for all flasks collected during BARCA-A. The emission ratios for biofuel burning ($\Delta CH_4/\Delta CO$ = 0.1369), tropical forest (0.1144), and savannah (0.0619) are represented by the slopes of the straight lines. (b) The vertical profiles for CH_4 and CO on the flight from Boa Vista to Manaus (Flt 5; BARCA-B) crossing a biomass burning plume. In the CH_4 profile, a ~70 ppb enhancement is notable while for CO the enhancement is much higher (~650 ppb).

1-sigma standard deviation of the vertical profiles in the eastern part for both campaigns due to higher oceanic influence. The higher 1-sigma standard deviation in the planetary boundary layer in the central part originates from several observed high CH_4 mixing ratios while ascending and descending to Manaus airport. In the western, central and northern part of the Amazon basin, CH_4 is higher at all altitudes during BARCA-B than during BARCA-A (21 ppb on average), which might be due to the expected enhanced CH_4 emissions from wetlands in May compared to November [*Devol et al.*, 1990].

3.2. Methane Source Identification

[18] To identify and distinguish the different main sources of CH_4 in the Amazon region (wetlands, biomass burning, and other anthropogenic emissions), we have used two techniques, i.e., the use of CO as a tracer for biomass burning and analysis of the isotopic composition of CH_4.

[19] During BARCA-A extensive biomass burning was going on in the Amazon River plain between Santarém and Belém, in the northeast region of Brazil, and along the southern edge of the Amazon basin. Figure 4a shows the distribution of the CH_4 mixing ratios as a function of CO mixing ratios during BARCA-A. The observations indicate that a large fraction of the flask samples contain a biomass burning signature, as identified by the high CO values. The slopes of the lines in Figure 4a correspond to the expected $\Delta CH_4/\Delta CO$ emission ratios for savanna, tropical forest, and biofuel burning after *Andreae and Merlet* [2001]. Some samples, especially flask J1420, collected on FLT 5 from Belém to Santarém (1.495°S, 48.728°W) at 2104 m altitude, clearly fall on this trend, which is evidence that biomass burning is the dominant source of the small CH_4 increase seen in this sample. The emission ratio in this sample relative to the regional background values measured on the same flight (flask J1416, CO = 176 ppb, CH_4 = 1786 ppb) is $\Delta CH_4/\Delta CO = 0.095$. A bivariate regression [*Cantrell*, 2008] of the CH_4 versus the CO mixing ratios from BARCA-A (excluding sample J1420 and the samples with CH_4 values >1850 ppb) yields a slope of 0.134, again consistent with the average emission ratio of 0.114 ± 0.020 of *Andreae and Merlet* [2001] for tropical forest burning. The low coefficient of determination, r^2 = 0.18, indicates, however, that only a minor fraction of the variance of CH_4 is explained by the contribution from biomass burning. Also during the end of the wet season (BARCA-B), a biomass burning event was sampled on FLT 5 from Boa Vista to Manaus (Figure 4b) with a calculated emission ratio of $\Delta CH_4/\Delta CO$ = 0.112 for the continuous data. In addition, the emission ratio of the flask sample J1429 $\Delta CH_4/\Delta CO$ = 0.102, collected while flying through this biomass burning plume, is consistent with the emission ratio derived from the continuous data and the values proposed in the literature for tropical forest burning.

[20] It is evident from Figure 4, however, that in most of the samples the observed CH_4 elevations are far stronger than what is expected from biomass burning, as they fall well above the straight lines in Figure 4a that indicate the predicted composition of samples resulting from the addition of biomass smoke to the air entering the Basin (ca. 1770 ppb CH_4 and 80 ppb CO). Therefore, although most of the flasks sampled during BARCA-A contain a biomass burning signature, this has only a minor influence on the observed CH_4 enhancements. In particular, all flasks with CH_4 mixing ratios >1850 ppb could be identified to have excess CH_4 of biogenic origin by isotope analysis. Figures 5a and 5b show the results of the isotope measurements in a Keeling plot, where the δ values are plotted as a function of the inverse of the mixing ratio. Also shown are isotope mixing lines that would result from contributions from single potentially important CH_4 sources. The y axis intercepts of δD = −312‰ for BARCA-A (Figure 5a) and $\delta^{13}CH_4$ = −58.8‰ for BARCA-B (Figure 5b) are in excellent agreement with what is expected from biogenic sources. Most of the flasks sampled during BARCA-B with CH_4 mixing ratios

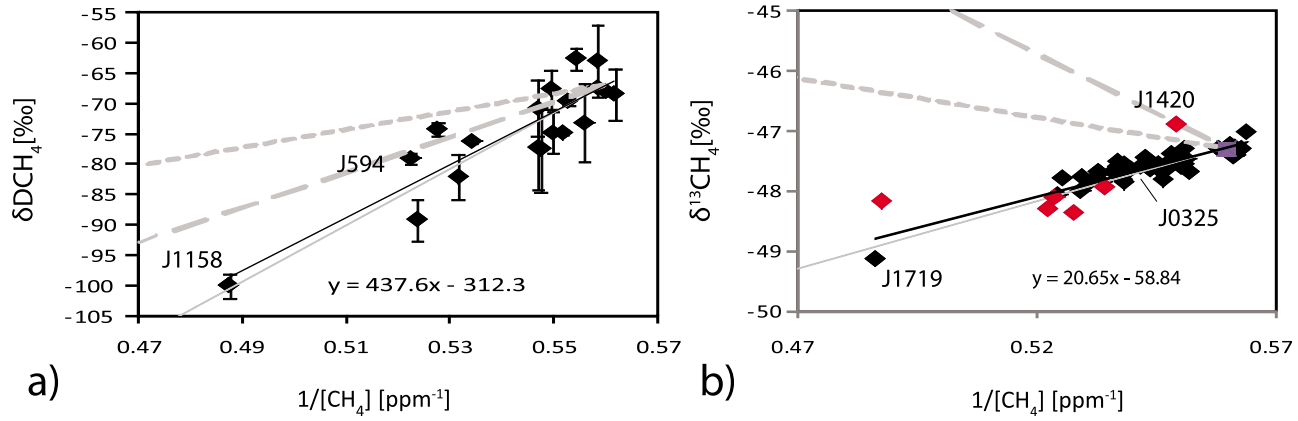

Figure 5. Keeling plot representation (δ value versus inverse mixing ratio) of the isotope measurement results obtained on selected flasks from BARCA-A and BARCA-B. (a) The δD signature for flask samples collected during BARCA-A; (b) the $\delta^{13}CH_4$ signature for flask samples collected during BARCA-A (red symbols) and BARCA-B (black symbols). Selected flasks include the ones with the highest mixing ratio, as well as some with the lowest and intermediate mixing ratios. Indicated in gray are isotope mixing lines for important CH_4 sources, namely biogenic CH_4, e.g., from tropical wetlands ($\delta^{13}CH_4 \sim -60‰$, $\delta D \sim -320‰$, solid line), CH_4 from thermogenic processes, e.g., natural gas and coal mining ($\delta^{13}CH_4 \sim -40‰$, $\delta D \sim -150‰$, dotted line), and CH_4 from biomass burning ($\delta^{13}CH_4 \sim -25‰$, $\delta D \sim -225‰$, dashed line). The black line indicates the fit of the observations using a linear regression model. Isotope source signatures are based on *Quay et al.* [1999].

>1850 ppb had been collected over wetland areas, for which calculated trajectories do not show urban influence. For example, flask J1719 was collected at 270 m altitude over an extensive wetland area (1.67°S, 51.32°W) (Figure 5b) and shows a measured CH_4 mixing ratio of 2055 ppb and a $\delta^{13}C$ signature of −49.1‰, in agreement with biogenic CH_4 emissions. It is clear that the majority of the isotopic measurements, both for BARCA-A and for BARCA-B, agree very well with biogenic methane being the dominant source responsible for the CH_4 elevations in the analyzed samples. The biogenic methane can be mainly attributed to CH_4 emissions from wetlands as the dominant biogenic source [*Bustamante et al.*, 2009].

[21] As described above, the $\Delta CH_4/\Delta CO$ emission ratio for sample J1420 strongly indicates that biomass burning is the main source of the additional CH_4, and this is fully confirmed by $\delta^{13}CH_4$ analysis (Figure 5b). A clear isotope enrichment is observed that can only be caused by CH_4 from biomass burning. Unfortunately, this is the only sample of this type that was selected for isotope analysis, but as stated above, the CH_4 elevations from biomass burning are generally small, and at the present precision isotope analysis can only identify sources when the elevations caused by this source are clearly above background levels.

[22] Surprisingly, δD and $\delta^{13}CH_4$ analysis of two flask samples collected during BARCA-A near major cities (J594-Santarém, J1158-Manaus; Figures 5a and 5b) also suggests strong biogenic CH_4 emission sources for these samples, while the calculated backward trajectories in both cases clearly indicate urban influence (not shown). The CH_4 mixing ratio is much higher than what can be explained by combustion or biomass burning processes given the concomitant CO values. Other CH_4 mixing ratio enhancements in the continuous measurements close to major cities (Manaus, Santarém, and Belém) could also be attributed to urban influence using backward trajectory calculations. As one example, the CH_4 mixing ratios obtained on FLT 15 during BARCA-B are presented in Figures 6a and 6b. The three peaks of the CH_4 mixing ratio time series (Figure 6a, green line) with maximum values of 1870 ppb, 1926 ppb and 1980 ppb, respectively, do not show corresponding increases in CO (Figure 6a, blue line), except for the last peak, which could be related to thermal combustion processes. The isotope analysis from flask J0325, collected within the first peak, indicates a biogenic CH_4 source (Figure 5b). A forward calculation of the propagation of the Manaus plume (released at the beginning of the flight) using the Stochastic Time Inverted Lagrangian Transport (STILT) model [*Lin et al.*, 2003] illustrates the influence area within the planetary boundary layer. Enhanced CH_4 mixing ratios are observed exactly at the locations where the flight path crosses the Manaus plume, which supports our hypothesis of biogenic CH_4 emissions from urban areas. However, CH_4 from anthropogenically driven biological processes, such as waste decomposition or cattle holding, cannot be readily distinguished from wetland emissions by isotope analysis. We suggest that such anthropogenic sources, or the recently reported CH_4 emissions from open sewers [*Guisasola et al.*, 2008], could be large contributors of CH_4 emissions in tropical cities. A plausible source is the decomposition of uncontrolled waste emissions into the waters of the densely populated sloughs along the Amazon River in Manaus and other urban areas. Thus, our observations suggest that the main anthropogenic CH_4 emissions from the city of Manaus are of biogenic origin.

4. Comparison to Global Models

[23] Model output from five different global TM5 inversions was compared to the CH_4 observations of BARCA-A

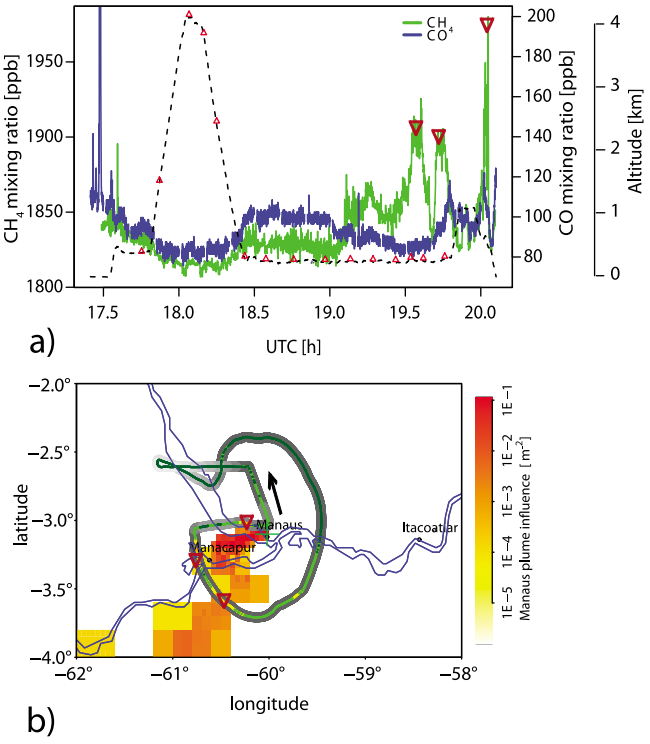

Figure 6. (a) Time series of Flt 15 around Manaus city during BARCA-B. The black dashed line indicates the altitude of the flight track and the small red triangles show the locations where flasks were collected. The big triangles denote the increase in the CH_4 mixing ratio while crossing the Manaus plume. (b) The distribution of the Manaus plume using a forward calculation of the Stochastic Time Inverted Lagrangian Transport (STILT) model and the flight track of Flt 15 around Manaus starting north (indicated by the black arrow). The gray color scale indicates the altitude of the flight track (light gray is high altitude (~3500–4000 m), dark gray is low altitude (~500 m)), and the overlying color scale denotes the magnitude of the CH_4 mixing ratio (green is low mixing ratio (~1800–1850 ppb) and orange is high mixing ratio (>1900 ppb)).

and BARCA-B: two versions of the model of *Bergamaschi et al.* [2009, 2010] (referred to as PB and PB-SCI, respectively) and two TM5 inversions from Houweling (referred to as SH and SH-SCI)—both with observational constraints from the NOAA-ESRL surface stations and the SCIAMACHY (SCI) satellite retrievals—and Carbon Tracker Methane (referred to as CT) using only NOAA-ESRL surface sites as observational constraints.

[24] The inversion is either performed by using the 4DVAR technique [*Meirink et al.*, 2008b] (PB, PB-SCI, SH, and SH-SCI) or Ensemble Kalman Filter (CT). Models PB and PB-SCI apply a semi-exponential PDF for the prior emissions to enforce that posterior emissions remain positive, and optimize four source categories independently (wetlands, rice, biomass burning, and other emission) [see *Bergamaschi et al.*, 2010]. For SH and SH-SCI only the total CH_4 flux is optimized, while CT also optimizes for four different source categories (natural emissions, biomass burning, fossil, and one category containing rice, waste, and agriculture emissions). Also the number of NOAA-ESRL surface stations from which observations are used in the inversion differs (cf. Table 2). The two inversions using SCIAMACHY satellite observations (PB-SCI and SH-SCI) differ in their way of accounting for the bias correction of the SCIAMACHY data by fitting a second-order polynomial function of latitude and month (PB-SCI), and fitting a function with a uniform scaling factor for the total column and a scalar accounting for air mass dependent errors as unknowns (SH-SCI). Both PB-SCI and SH-SCI use the new IMAPv5.5 SCIAMACHY retrievals [*Frankenberg et al.*, 2011], which enable consistent CH_4 retrievals from 2003 through 2009 despite the significant SCIAMACHY pixel degradation within the CH_4 $2\nu3$ band occurring at the end of 2005. However, these new IMAPv5.5 retrievals have systematically higher values in the tropics than the previous IMAPv5.0 retrievals available for the period 2003–2005 [*Frankenberg et al.*, 2008, 2011]. An overview over the main characteristics of each model (or model simulation, respectively) is found in Table 2.

[25] The global models are all based on the same underlying transport model TM5 [*Krol et al.*, 2005], but use different prior input CH_4 fluxes from wetlands: the Kaplan inventory [*Bergamaschi et al.*, 2007] for PB and PB-SCI, the LPJ-WhyME model [*Wania*, 2007] for SH and SH-SCI, and wetland fluxes based on *Matthews and Fung* [1987] for CT. Both TM5 inversions from *Bergamaschi et al.* [2009] use the same prior fluxes (referred to AP-PB from here on). The prior fluxes of both inversions of Houweling are denoted as AP-SH (and AP-CT for prior fluxes of CT). For AP-CT, the spatial distribution of the prior wetland CH_4 fluxes is constant throughout the year and only the magnitude of the prior CH_4 wetland emission changes in time. On the other hand, AP-PB and AP-SH have the spatial distribution of the wetland area changing in time between November 2008 and May 2009. In comparison to the prior wetland CH_4 emissions of AP-SH, AP-PB has lower wetland prior emissions in the region between Manaus and Santarem and higher emissions close to the Amazon delta. The wetland prior fluxes of AP-CT in the northern and northwestern part of the Amazon show mostly zero emissions (not shown). The biomass burning prior fluxes of all three models are based on the Global Fire Emission Database, Version 2 (GFEDv2) [*van der Werf et al.*, 2004], but differ in their temporal resolution. AP-PB and AP-SH use monthly averages of biomass burning emissions. AP-PB utilizes here for the averages of fire emissions from the years 1997–2007. AP-SH takes the monthly averages of the year 2008 also for the year 2009. AP-CT uses daily fire emissions interpolated from monthly averages of the corresponding years 2008 and 2009. For May 2009, a comparison of the prior biomass burning emissions of all models does not show any significant differences in the central Amazon basin, while for November 2008 AP-SH does not capture biomass burning emissions in the eastern part of the Amazon, while the other two biomass burning prior fluxes do (also not shown). To compare the CH_4 values of the global model simulations to the BARCA CH_4 airborne measurements, the CH_4 model values were extracted from $6^\circ \times 4^\circ$ 3 hourly gridded fields at the observation location (flask location for BARCA-A, measurement location every 3-s for BARCA-B) by using a three-dimensional interpolation routine and additionally temporal interpolation. The extracted values were binned into 500-m vertical intervals

Table 2. Overview Over the Differences Between the Five TM5 Model Simulations Used for Comparison With the BARCA Observations (PB, PB-SCI, SH, SH-SCI, and CT)[a]

	PB-SCI	PB	SH-SCI	SH	CT
			Prior Fluxes		
Wetlands	'JK' inventory [*Bergamaschi et al.*, 2007]	'JK' inventory [*Bergamaschi et al.*, 2007]	LPJ-WhyME [*Wania*, 2007]	LPJ-WhyME [*Wania*, 2007]	*Matthews and Fung* [1987]
Biomass burning	GFEDv2 [*van der Werf et al.*, 2004] (average 1997–2007)	GFEDv2 [*van der Werf et al.*, 2004] (average 1997–2007)	GFEDv2 [*van der Werf et al.*, 2004] (2008)	GFEDv2 [*van der Werf et al.*, 2004] (2008)	GFEDv2 [*van der Werf et al.*, 2004] (2008, 2009)
Anthropogenic emissions	EDGARV4.0 (S. Monni et al., manuscript in preparation, 2010)	EDGARV4.0 (S. Monni et al., manuscript in preparation, 2010)	EDGARV4.0 Extrapolated using BP statistics [*Olivier and Berdowski*, 2001]	EDGARV4.0 Extrapolated using BP statistics [*Olivier and Berdowski*, 2001]	EDGAR 3 [*Olivier and Berdowski*, 2001]
			Model Setup		
Inversion technique	4DVAR	4DVAR	4DVAR	4DVAR	Ensemble Kalman Filter
Number of NOAA surface stations	32	32	46	46	80
SCIAMACHY retrieval	IMAP V5.5 [*Frankenberg et al.*, 2011]	-	IMAP V5.5 [*Frankenberg et al.*, 2011]	-	-
Meteorology	ECMWF ERA interim	ECMWF ERA interim	ECMWF ERA interim	ECMWF ERA interim	ECMWF operational
Horizontal resolution	6° × 4°	6° × 4°	6° × 4°	6° × 4°	6° × 4°
Number of vertical layers	25	25	25	25	25
OH fields	Carbon Bond Mechanism 4 (CBM-4)	Carbon Bond Mechanism 4 (CBM-4)	*Spivakovsky et al.* [2000]	*Spivakovsky et al.* [2000]	*Spivakovsky et al.* [2000]
Runtime period	15 months	15 months	01/2007–12/2009	01/2007–12/2009	01/2000–12/2009

[a]The source of prior fluxes for the most important CH_4 emission sources, the number of NOAA-ESRL surface stations used for the inversion, the version of the SCIAMACHY retrievals (for PB-SCI and SH-SCI), and basic information is shown.

and separated for different regions of the Amazon basin as already described for the observations in section 3.1 (Figure 3).

[26] For BARCA-A (Figures 7a–7f, number 1), the vertical profiles of the model simulations from inversions using SCIAMACHY observations show clearly higher mixing ratios than the inversions using only observations from NOAA-ESRL surface stations (except for CT in the free troposphere). Both profiles (PB-SCI and SH-SCI) agree well with each other and overestimate the observations by ~10 ppb except for the eastern part (cf. Figure 7e1). In the eastern part, their disagreement with the observations in the planetary boundary layer is highest. SCIAMACHY observations are rather insensitive to biomass burning, because the CH_4/CO_2 ratio used in the retrievals is similar for background air and biomass burning [see *Petersen et al.*, 2010]. This fact could be a plausible explanation for the lower CH_4 mixing ratios of both models using SCIAMACHY observations in the eastern part. Surprisingly, SH-SCI shows higher mixing ratios in the planetary boundary layer even though the prior biomass burning emissions depict almost no emission in that region. Therefore, higher wetland prior emissions of AP-SH as compared to AP-PB between Manaus and Santarém could be a reasonable explanation for this. The deviation from the observed vertical profiles for all simulations is highest in the eastern part during BARCA-A, which could be due to underestimated wetland emissions and biomass burning activity of all models in that region. In general for BARCA-A, the vertical profiles of the simulations using observations only from NOAA-ESRL surface stations for their inversion system have the tendency to underestimate the observed mixing ratios, SH more than PB and CT. In the free troposphere CT is closest to the observations and surprisingly overestimates the observations (except for the eastern part) on average by 7 ppb, but underestimates the observations especially in the planetary boundary layer. One reason therefore lies in much lower posterior fluxes of CT compared to all other models. In general for BARCA-A, the comparison clearly illustrates the benefit of using SCIAMACHY observations in the inversion as those fit the observations better on average (5–6 ppb overall bias for PB-SCI and SH-SCI compared to 11–17 ppb bias for PB, SH, and CT) as clearly illustrated in Figure 7a1.

[27] For BARCA-B (Figures 7a–7f, number 2), the situation is more complex: In contrast to BARCA-A, the simulations of the SCIAMACHY based inversions do not always show higher mixing ratios throughout the total vertical profile for all regions when compared to simulations of the same models using constraints from NOAA-ESRL surface stations only in the inversion. In the free troposphere (except for the western part), the simulations of SCIAMACHY-based inversions PB-SCI and SH-SCI generally fit the observed mixing ratios well (bias <10 ppb). This applies also for CT (except for the southern part), which is constrained only by NOAA-ESRL surface stations. However, SH-SCI and SH have the highest mixing ratios in the planetary boundary layer, contrary to the results for BARCA-A, where the SCIAMACHY based inversions PB-SCI and SH-SCI always show the highest CH_4 mixing ratios. The mixing ratios of PB-SCI and PB in the planetary boundary layer are significantly lower (western, central, and eastern part) in comparison to mixing ratios of SH and SH-SCI during BARCA-B. This suggests that the distribution of the wetland prior emission patterns has a stronger impact on the simulated mixing ratios in the planetary boundary layer for BARCA-B than for BARCA-A, even though differences in the weight of the prior between the different models could be a possible reason. Interestingly, the CH_4 mixing ratios in the western part (and partially also in the northern part) at altitudes between 3000 m and 4000 m are enhanced compared to the other regions of the Amazon basin, which is not captured well by any of the models. This points to a larger source from a greater distance and indeed, calculations of backward trajectories for these days at the corresponding altitudes indicate contributions from the northwestern part of South America, a region where also SCIAMACHY sees high CH_4 mixing ratios [*Frankenberg et al.*, 2006, 2011]. This suggests that the atmospheric region influencing the Amazon basin is considerably larger than the Amazon basin itself.

[28] The differences between each model and the observations for the different sampling regions are likely related to differing posterior flux distributions. To assess this, a closer look was taken at the posterior fluxes within the surface area influencing the respective sampling regions. In order to obtain the influence regions of the Amazon basin during BARCA-A and BARCA-B, footprint calculations, describing the sensitivity of atmospheric mixing ratio observations to upstream surface fluxes, have been carried out using the STILT model for each flask observation during BARCA-A and roughly four observations per flown vertical profile during BARCA-B. They were calculated 10 days backward in time and temporally integrated for each sampling region (cf. Figure A1). 3-h ECMWF meteorological fields were used for the calculation and it was performed on a $6^\circ \times 4^\circ$ horizontal grid (same as the grid of the posterior fluxes) to minimize the differences in the representation of the atmospheric transport between STILT and TM5. Figure 8 illustrates the monthly budgets for BARCA-A (Figure 8a) and BARCA-B (Figure 8b) as function of the mean bias of the vertical profiles as illustrated in Figure 7. The CH_4 flux for each sampling region $k = 1,5$ for the total land fraction of the STILT domain (cf. Figure A1), is weighted by the relative influence from integrated footprints per sampling region using the following formula:

$$monthly\_budget_k = \Sigma_{n=1,n_k} \Sigma_{(i,j)\mathrm{land}} \frac{flux[i,j] \times FP_k^{[n]}[i,j]}{TFP}. \quad (1)$$

[29] Here, $monthly\_budget_k$ indicates the derived monthly budget for the corresponding sampling region k as illustrated in Figures 8a and 8b, *flux* the CH_4 posterior flux of the TM5 simulations of each land grid cell [*i,j*], *FP* the value of each single footprint with receptor location in the sampling region k (sum over the total number of n_k footprints with receptor location in the corresponding sampling region), and *TFP* the value of the total integrated campaign footprint that is calculated as follows:

$$TFP = \Sigma_{k=1,5} \Sigma_{n=1,n_k} \Sigma_{(i,j)\mathrm{land}} FP_k^{[n]}[i,j]. \quad (2)$$

[30] The obtained relationship between monthly CH_4 budget and bias of the vertical profile indicates an almost linear relation between the model-observation mismatch and

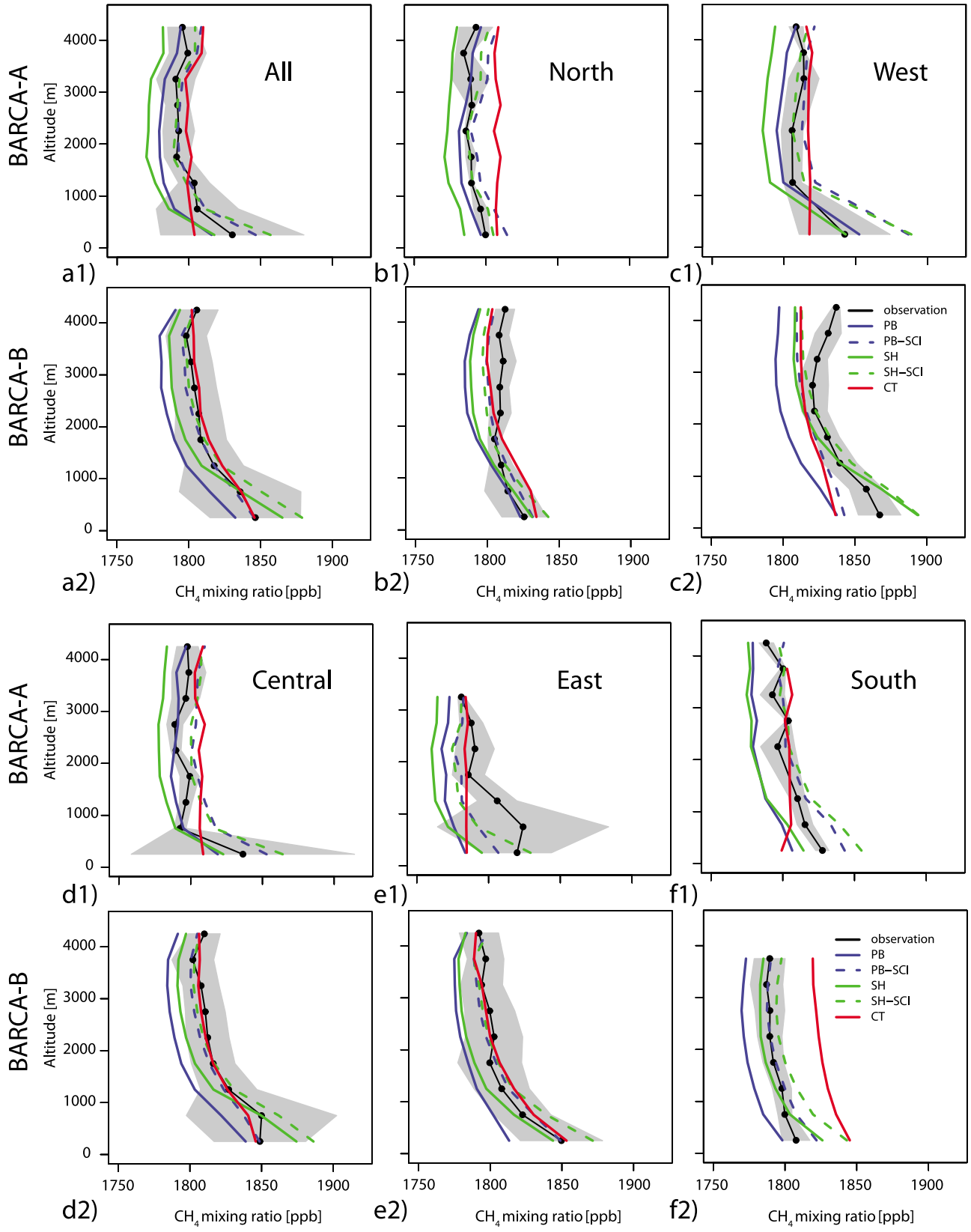

Figure 7. Five-hundred-meter binned vertical profiles for the observed CH_4 mixing ratios and the modeled CH_4 mixing ratios for (a) the total campaign average and (b–f) different regions of the Amazon basin (cf. Figure 1b). The mean vertical profiles are shown for (1) BARCA-A and (2) BARCA-B, and the 1-sigma standard deviation of the observations is denoted as a gray shaded area.

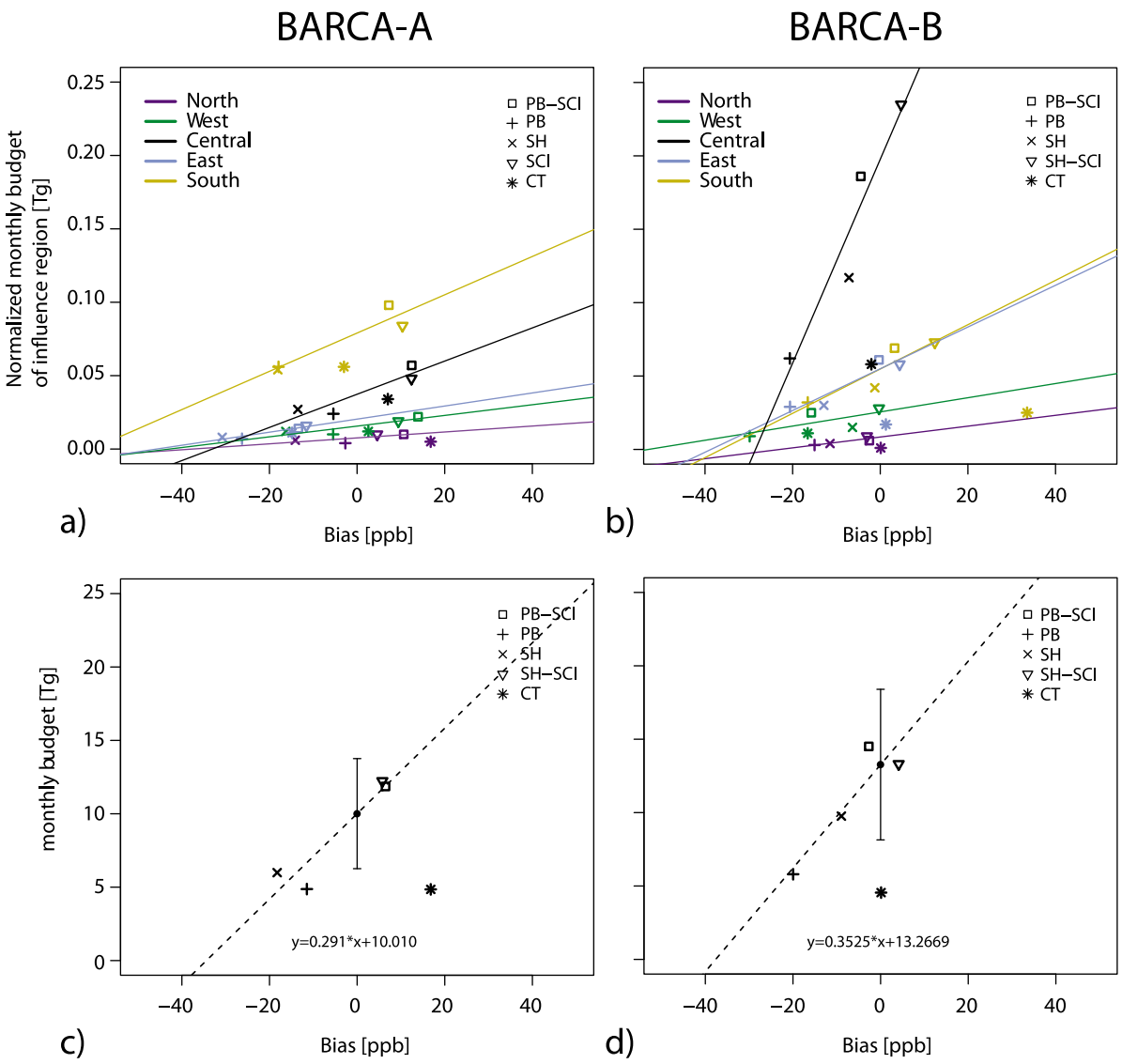

Figure 8. (a and b) The monthly budget for each of the five TM5 based global CH_4 inversions, determined for the influence regions (cf. Figure A1) derived from the STILT model, as a function of the model-observation mismatch (bias) of the vertical profiles for each of the five different sampling regions. The points are colored accordingly to the corresponding sampling regions (yellow, south; green, west; violet, north; blue, east; black, central) (cf. Figures 1a and 1b). Colored lines correspond to linear regressions within each region with correlation coefficients ranging from 0.72 to 0.96. Note that CT was not included in the calculation of the linear regressions. The monthly budget of the land fraction of the STILT domain (cf. Figure A1) is depicted as a function of the mean weighted bias (weighting accordingly to the fraction of the influence region) for (c) November 2008 and (d) May 2009 for each of the five models. The black dot denotes the "best budget estimate" obtained for bias = 0, and the error bars illustrate the 95% confidence interval (CT also not included here).

the calculated monthly CH_4 budget of the influence region. However, CT clearly does not fall on the trend. Possible reasons that influence the bias are the above described differences in the CH_4 fluxes over land, differences in the atmospheric background mixing ratio upstream of the continent, and differences in the vertical distribution. For CT, differences of 18 ppb (BARCA-A) to 36 ppb (BARCA-B) were found in the background CH_4 mixing ratio upstream of the South American continent compared to the other four inversions, which show a maximum difference of 3 ppb among themselves. Besides potential differences in the vertical distribution, which cannot be excluded, this might be an explanation why CT does not fall on the trend. Therefore, we do not include CT in the calculations of the linear regression. The correlation coefficients of the linear regression range from r = 0.72 (north) to 0.95 (east) for BARCA-A (a) and from r = 0.70 (west) to 0.96 (central) for BARCA-B (b). The slope of the lines in Figures 8a and 8b increases with increased relative influence of the footprints or higher budget of the corresponding influence region (see equation (1)). For

BARCA-A, the southern and central parts show the highest slopes. Due to the high number of observations in the central part, the relative influence of the footprint is higher compared to other regions (also true for BARCA-B). The influence region of the southern region during BARCA-A is mainly located over the South American continent leading to higher budget number in comparison to other regions. In the northern part the budget numbers are very low for both campaigns, because most of the surface influence area is located over the ocean. For BARCA-A (except for the northern part), the inversions using SCIAMACHY observations show in general a more positive bias in the model-observation mismatch of the vertical profile and higher monthly CH_4 budgets compared to inversions using only observations from NOAA surface stations, which is not clearly seen for BARCA-B, as already discussed above. Figures 8c and 8d demonstrate the total monthly budget (sum over the monthly emissions of all land grid cells of the STILT domain, not weighted) as function of the mean weighted model-observation mismatch for all five TM5-based inversion systems during BARCA-A (Figure 8c) and BARCA-B (Figure 8d). Weighting of the mean model-observation mismatch from all five sampling regions k (*mean_bias*) was calculated accordingly to:

$$mean\_bias = \Sigma_{k=1,5} \frac{bias[k] \times \Sigma_{n=1,n_k} FP_k^{[n]}}{TFP} \quad (3)$$

with *bias* being the model-observation mismatch of the corresponding sampling region k. From the linear fit illustrated in Figures 8c and 8d (note that CT is also not included in the linear fit), the monthly CH_4 budget for the total land fraction of the STILT domain for bias = 0 is obtained at 10.5 Tg for November 2008 and at 13.3 Tg for May 2009 with a 95% confidence interval of the linear fit ranging from 6.3 Tg to 13.8 Tg for November 2008 and 8.1 Tg to 18.4 Tg for May 2009. The fraction emitted by the Amazon lowland region (<500 m) as described in *Melack et al.* [2004] is calculated to 0.57 $\pm$ 0.14 (1-sigma standard deviation resulting from differences in the spatial flux patterns between models) for BARCA-A, and to 0.51 $\pm$ 0.17 for BARCA-B. By multiplication of this fraction with the obtained monthly CH_4 budgets for bias = 0 in Figures 8c and 8d and division by the area of the Amazon lowland region, the CH_4 flux strength of the Amazon lowland region is estimated to 36 $\pm$ 12 mg m^2 d^{-1} for BARCA-A and 43 $\pm$ 18 mg m^2 d^{-1} for BARCA-B using quadratic error propagation (29 $\pm$ 12 mg m^2 d^{-1} for BARCA-A and 34 $\pm$ 19 mg m^2 d^{-1} for BARCA-B if CT is included in the calculations). Our flux estimates derived for the Amazon lowland region agree well with the numbers found by *Miller et al.* [2007] who proposed 35 mg m^2 d^{-1} as multiannual averaged CH_4 flux estimates for the Santarém area and 20 mg m^2 d^{-1} for the Manaus area.

[31] The obtained annual CH_4 budget of 2008 and 2009 for the Amazon lowland region for the different model simulations ranges from 33 Tg to 42 Tg for PB, PB-SCI, SH and SH-SCI and 17–18 Tg for CT. Compared to *Melack et al.* [2004] who suggested a number of 29.3 Tg for the annual CH_4 wetland emissions in the Amazon lowland region, the TM5 based global inversions (except for CT) have the tendency to estimate up to 7 Tg higher CH_4 wetland fluxes under the assumption that 80–90% of the total fluxes are originating from wetlands (calculated from the optimized posterior fluxes of PB-SCI, PB, and CT) throughout the whole year. As no linear relationship between the calculated annual budget numbers of all five TM5-based inversions, both for 2008 and 2009, and the model data mismatch of the two BARCA campaigns could be found, we conclude that it is very difficult to obtain a reliable estimate of an annual CH_4 budget number of the Amazon region based on the model-observation mismatch with only two months data coverage per year, as obtained during the two BARCA campaigns, considering the different seasonal variation of the posterior fluxes of the different TM5 models.

5. Conclusions

[32] The data set presented here, with over 150 vertical profiles from 27 flights across the Amazon basin during two time periods at the end of the dry season in November 2008 and the end of the wet season in May 2009, gives an impressive overview over the CH_4 distribution in the lower troposphere in that region, which can be used to validate and evaluate models (the data set is available on request via e-mail to swofsy@seas.harvard.edu).

[33] Using SF_6 as hemispheric tracer allowed us to trace the incoming air into the Amazon basin back to be dominantly of Southern hemispheric origin during BARCA-A and a mixture of both hemispheres during BARCA-B. With the help of isotope analysis we confirmed that the dominant part of the CH_4 emissions can be attributed to biogenic origin. CH_4 emissions of major cities are found to have a major contribution from biogenic origin, e.g., sewage gas. During BARCA-A, a minor part of the CH_4 emissions could be identified to originate from biomass burning using CO as an additional tracer.

[34] By comparing the observations to five TM5-based global CH_4 inversions, we found that the inversions using SCIAMACHY satellite retrievals match the observations better during both campaigns. Except for the western part of the Amazon region, PB-SCI was found to be very consistent with the observations during BARCA-B. Comparing the monthly CH_4 budgets of the land influence regions of the Amazon basin, calculated via a LPDM, to the observed model-observation mismatch allowed us to estimate the source strength of the Amazon lowland basin to 36 $\pm$ 12 mg m^{-2} d^{-1} during BARCA-A and 43 $\pm$ 18 mg m^{-2} d^{-1} during BARCA-B. In our case the model-observation mismatch could be attributed to the characteristics of the monthly CH_4 budget, but not on the yearly timescale. Thus, we conclude that for obtaining a robust and reliable annual CH_4 budget for the Amazon region, conducting such aircraft campaigns, on a regional scale and at regular time intervals is essential during the whole year.

Appendix A

[35] Footprint calculations for the BARCA observations in the five different sampling regions were conducted to obtain information on the influence regions of the Amazon basin. The footprints were calculated on a 6° × 4° horizontal grid 10 days backward in time using 3-h ECMWF meteorological fields. The temporally integrated footprints for each sampling region are shown in Figure A1.

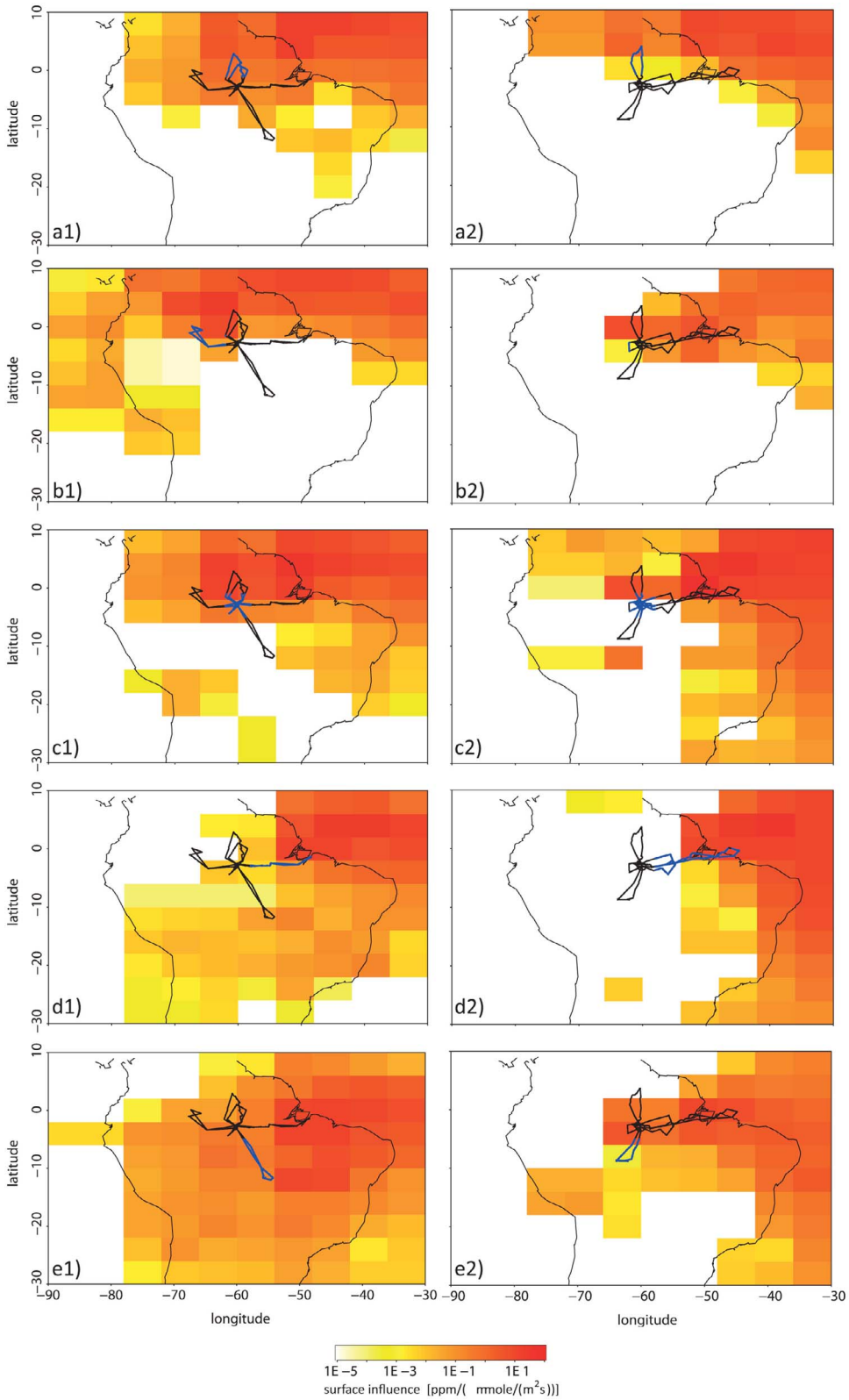

Figure A1. Integrated footprints (describing the sensitivity of atmospheric mixing ratio measurements to upstream surface-atmosphere fluxes) for all flask observations obtained in the corresponding sampling regions ((a) north, (b) west, (c) central, (d) east, (e) south) during (1) BARCA-A and roughly four equally distributed observation per flown vertical profile for (2) BARCA-B. The flight track of each airborne campaign is colored in black, while the part of the flight track that corresponds to the respective sampling region is colored in blue.

[36] **Acknowledgments.** We are very thankful to all the other BARCA team members, namely E. Gottlieb, V. Y. Chow, M. D. P. Longo, G. W. Santoni, K. T. Wiedemann, F. Morais, A. C. Ribeiro, N. Jürgens, M. Bela, L. V. Gatti, J. B. Miller, and the two pilots of the INPE Bandeirante airplane, P. Celso and D. Gramacho. We thank E. J. Dlugokencky for permission to use unpublished SF_6 and CH_4 data from the NOAA ESRL stations. We also would like to thank Armin Jordan, who did the flask measurements, and Stephan Baum, who also took care of the flasks, and Silvana Schott for assistance with graphics. We thank two anonymous reviewers for improvements on the manuscript. This work was supported by the Max Planck Society. Funding for the BARCA flights was provided by Max Planck Society, NASA through the grants NASA NNX08AP68A and NASA NNX10AR75G, the CNPq Millennium Institute of the Large Scale Biosphere–Atmosphere Experiment in Amazonia (LBA), and FAPESP. We thank INPA (Instituto Nacional de Pesquisas da Amazonia) for the support for the LBA central office.

References

Andreae, M. O., and P. Merlet (2001), Emission of trace gases and aerosols from biomass burning, *Global Biogeochem. Cycles*, *15*(4), 955–966, doi:10.1029/2000GB001382.

Andreae, M. O., P. Artaxo, V. Beck, M. Bela, C. Gerbig, K. Longo, J. W. Munger, K. T. Wiedemann, and S. C. Wofsy (2012), Carbon monoxide and related trace gases and aerosols over the Amazon basin during wet and dry seasons, *Atmos. Chem. Phys. Discuss.*, *12*, 8107–8168, doi:10.5194/acpd-12-8107-2012.

Bartlett, K. B., and R. C. Harriss (1993), Review and assessment of methane emissions from wetlands, *Chemosphere*, *26*, 261–320, doi:10.1016/0045-6535(93)90427-7.

Bartlett, K. B., P. M. Crill, J. A. Bonassi, J. E. Richey, and R. C. Harriss (1990), Methane flux from the Amazon River floodplain: Emission during rising water, *J. Geophys. Res.*, *95*(D10), 16,773–16,788, doi:10.1029/JD095iD10p16773.

Bergamaschi, P., et al. (2007), Satellite chartography of atmospheric methane from SCIAMACHY onboard ENVISAT: 2. Evaluation based on inverse model simulations, *J. Geophys. Res.*, *112*, D02304, doi:10.1029/2006JD007268.

Bergamaschi, P., et al. (2009), Inverse modeling of global and regional CH_4 emissions using SCIAMACHY satellite retrievals, *J. Geophys. Res.*, *114*, D22301, doi:10.1029/2009JD012287.

Bergamaschi, P., et al. (2010), Inverse modeling of European CH_4 emissions 2001–2006, *J. Geophys. Res.*, *115*, D22309, doi:10.1029/2010JD014180.

Bousquet, P., et al. (2006), Contribution of anthropogenic and natural sources to atmospheric methane variability, *Nature*, *443*(7110), 439–443, doi:10.1038/nature05132.

Brass, M., and T. Röckmann (2010), Continuous-flow isotope ratio mass spectrometry method for carbon and hydrogen measurements on atmospheric methane, *Atmos. Meas. Tech.*, *3*, 1707–1721, doi:10.5194/amt-3-1707-2010.

Bustamante, M. M. C., M. Keller, and D. A. Silva (2009), Sources and sinks of trace gases in Amazonia and the Cerrado, in *Amazonia and Global Change*, *Geophys. Monogr. Ser*, vol. 186, edited by M. Keller et al., pp. 337–354, AGU, Washington, D. C., doi:10.1029/2008GM000733.

Cantrell, C. A. (2008), Technical note: Review of methods for linear least-squares fitting of data and application to atmospheric chemistry problems, *Atmos. Chem. Phys.*, *8*, 5477–5487, doi:10.5194/acp-8-5477-2008.

Carmo, J. B., M. Keller, J. D. Dias, P. B. Camargo, and P. Crill (2006), A source of methane from upland forests in the Brazilian Amazon, *Geophys. Res. Lett.*, *33*, L04809, doi:10.1029/2005GL025436.

Chen, H. (2010), Development of a high-accuracy continuous CO_2/CH_4/H_2O analyzer for deployment on board a commercial airliner, PhD thesis, 186 pp., Friedrich Schiller Univ. Jena, Germany.

Chen, H., et al. (2010), High-accuracy continuous airborne measurements of greenhouse gases (CO_2 and CH_4) using the cavity ring-down spectroscopy (CRDS) technique, *Atmos. Meas. Tech.*, *3*, 375–386, doi:10.5194/amt-3-375-2010.

Crill, P. M., K. B. Bartlett, J. O. Wilson, D. I. Sebacher, R. C. Harriss, J. M. Melack, S. MacIntyre, L. Lesack, and L. Smith-Morrill (1988), Tropospheric methane from an Amazonian foodplain lake, *J. Geophys. Res.*, *93*(D2), 1564–1570, doi:10.1029/JD093iD02p01564.

Devol, A. H., J. E. Richey, W. A. Clark, S. L. King, and L. A. Martinelli (1988), Methane emission to the troposphere from the Amazon floodplain, *J. Geophys. Res.*, *93*(D2), 1583–1592, doi:10.1029/JD093iD02p01583.

Devol, A. H., J. E. Richey, B. R. Forsberg, and L. A. Martinelli (1990), Seasonal dynamics in methane emissions from the Amazon River floodplain to the troposphere, *J. Geophys. Res.*, *95*(D10), 16,417–16,426, doi:10.1029/JD095iD10p16417.

Dlugokencky, E. J., R. C. Myers, P. M. Lang, K. A. Masarie, A. M. Crotwell, K. W. Thoning, B. D. Hall, J. W. Elkins, and L. P. Steele (2005), Conversion of NOAA atmospheric dry air CH_4 mole fractions to a gravimetrically prepared standard scale, *J. Geophys. Res.*, *110*, D18306, doi:10.1029/2005JD006035.

Dlugokencky, E. J., P. M. Lang, and K. A. Masarie (2010), Atmospheric methane dry air mole fractions from the NOAA ESRL Carbon Cycle Cooperative Global Air Sampling Network, 1983–2009, version 2010–08–12, ftp://ftp.cmdl.noaa.gov/ccg/ch4/flask/event/, NOAA ESRL, Boulder, Colo.

Ferek, R. J., J. S. Reid, P. V. Hobbs, D. R. Blake, and C. Liousse (1998), Emission factors of hydrocarbons, halocarbons, trace gases and particles from biomass burning in Brazil, *J. Geophys. Res.*, *103*(32), 107–132.

Frankenberg, C., J. F. Meirink, M. van Weele, U. Platt, and T. Wagner (2005), Assessing methane emissions from global space-borne observations, *Science*, *308*(5724), 1010–1014, doi:10.1126/science.1106644.

Frankenberg, C., J. F. Meirink, P. Bergamaschi, A. P. H. Goede, M. Heimann, S. Körner, U. Platt, M. van der Weele, and T. Wagner (2006), Satellite chartography of atmospheric methane from SCIAMACHY onboard ENVISAT: Analysis of the years 2003 and 2004, *J. Geophys. Res.*, *111*, D07303, doi:10.1029/2005JD006235.

Frankenberg, C., P. Bergamaschi, A. Butz, S. Houweling, J. F. Meirink, J. Notholt, A. K. Petersen, H. Schrijver, T. Warneke, and I. Aben (2008), Tropical methane emissions: A revised view from SCIAMACHY onboard ENVISAT, *Geophys. Res. Lett.*, *35*, L15811, doi:10.1029/2008GL034300.

Frankenberg, C., I. Aben, P. Bergamaschi, E. J. Dlugokenchy, R. van Hees, S. Houweling, P. van der Meer, R. Snel, and P. Tol (2011), Global column-averaged methane mixing ratios from 2003 to 2009 as derived from SCIAMACHY: Trends and variability, *J. Geophys. Res.*, *116*, D04302, doi:10.1029/2010JD014849.

Guisasola, A., D. de Haas, J. Keller, and Z. Yuan (2008), Methane formation in sewer systems, *Water Res.*, *42*, 1421–1430, doi:10.1016/j.watres.2007.10.014.

Guyon, P., et al. (2005), Airborne measurements of trace gas and aerosol particle emissions from biomass burning in Amazonia, *Atmos. Chem. Phys.*, *5*, 2989–3002, doi:10.5194/acp-5-2989-2005.

Intergovernmental Panel on Climate Change (2007), *Climate Change 2007: The Physical Science Basis. Contribution of Working Group I to the Fourth Assessment Report of the Intergovernmental Panel on Climate Change*, edited by S. Solomon et al., Cambridge Univ. Press, New York.

Keller, M., M. Bustamante, J. Gash, and P. Silva Dias (Eds.) (2009), *Amazonia and Global Change*, *Geophys. Monogr. Ser*, vol. 186, 565 pp., AGU, Washington, D. C., doi:10.1029/GM186.

Keppler, F., J. T. G. Hamilton, M. Braß, and T. Röckmann (2006), Methane emission from terrestrial plants under aerobic conditions, *Nature*, *439*(7073), 187–191, doi:10.1038/nature04420.

Krol, M. C., S. Houweling, B. Bregman, M. van den Broek, A. Segers, P. van Velthoven, W. Peters, F. Dentener, and P. Bergamaschi (2005), The two-way nested global chemistry-transport zoom model TM5: Algorithm and applications, *Atmos. Chem. Phys.*, *5*, 417–432, doi:10.5194/acp-5-417-2005.

Lin, J. C., C. Gerbig, S. C. Wofsy, A. E. Andrews, B. C. Daube, K. J. Davis, and C. A. Grainger (2003), A near-field tool for simulating the upstream influence of atmospheric observations: The Stochastic Time-Inverted Lagrangian Transport (STILT) model, *J. Geophys. Res.*, *108*(D16), 4493, doi:10.1029/2002JD003161.

Lloyd, J., et al. (2007), An airborne regional carbon balance for Central Amazonia, *Biogeosciences*, *4*, 759–768, doi:10.5194/bg-4-759-2007.

Martinson, G. O., F. A. Werner, C. Scherber, R. Conrad, M. D. Corre, H. Flessa, K. Wolf, M. Klose, S. R. Gradstein, and E. Veldkamp (2010), Methane emissions from tank bromeliads in neotropical forests, *Nat. Geosci.*, *3*, 766–769, doi:10.1038/ngeo980.

Matthews, E., and I. Fung (1987), Methane emissions from natural wetlands: Global distribution, area, and environmental characteristics and sources, *Global Biogeochem. Cycles*, *1*(1), 61–86, doi:10.1029/GB001i001p00061.

Meirink, J. F., et al. (2008a), Four-dimensional variational data assimilation for inverse modeling of atmospheric methane emissions: Analysis of SCIAMACHY observations, *J. Geophys. Res.*, *113*, D17301, doi:10.1029/2007JD009740.

Meirink, J. F., P. Bergamaschi, and M. C. Krol (2008b), Four-dimensional variational data assimilation for inverse modeling of atmospheric methane emissions: Method and comparison with synthesis inversion, *Atmos. Chem. Phys.*, *8*, 6341–6353, doi:10.5194/acp-8-6341-2008.

Melack, J. M., L. L. Hess, M. Gastil, B. R. Forsberg, S. K. Hamilton, I. B. T. Lima, and E. Novo (2004), Regionalization of methane emissions

in the Amazon basin with microwave remote sensing, *Global Change Biol.*, *10*(5), 530–544, doi:10.1111/j.1365-2486.2004.00763.x.

Miller, J. B., L. V. Gatti, M. T. S. d'Amelio, A. M. Crotwell, E. J. Dlugokencky, P. Bakwin, P. Artaxo, and P. P. Tans (2007), Airborne measurements indicate large methane emissions from the eastern Amazon basin, *Geophys. Res. Lett.*, *34*, L10809, doi:10.1029/2006GL029213.

Nisbet, R. E. R., et al. (2009), Emission of methane from plants, *Proc. R. Soc. London, Ser. B*, *276*, 1347–1354, doi:10.1098/rspb.2008.1731.

Olivier, J. G. J., and J. J. M. Berdowski (2001), Global emissions sources and sinks, in *The Climate System*, edited by J. J. M. Berdowski et al., pp. 33–78, A. A. Balkema, Lisse, Netherlands.

Olivier, J. G. J., A. F. Bouwman, J. J. M. Berdowski, C. Veldt, J. P. J. Bloss, A. H. J. Visschedijj, C. W. M. van de Maas, and P. Y. J. Zandweld (1999), Sectoral emission inventories of greenhouse gases for 1990 on per country basis as well as 10 × 10, *Environ. Sci. Policy*, *2*, 241–263, doi:10.1016/S1462-9011(99)00027-1.

Petersen, A. K., T. Warneke, C. Frankenberg, P. Bergamaschi, C. Gerbig, J. Notholt, M. Buchwitz, O. Schneising, and O. Schrems (2010), First ground-based FTIR observations of methane in the inner tropics over several years, *Atmos. Chem. Phys.*, *10*, 7231–7239, doi:10.5194/acp-10-7231-2010.

Quay, P., J. Stutsman, D. Wilbur, A. Snover, E. Dlugokenchy, and T. Brown (1999), The isotopic composition of atmospheric methane, *Global Biogeochem. Cycles*, *13*(2), 445–461, doi:10.1029/1998GB900006.

Querino, C. A. S., C. J. P. P. Smeets, I. Vigano, R. Holzinger, V. Moura, L. V. Gatti, A. Martinewski, A. O. Manzi, A. C. de Araújo, and T. Röckmann (2011), Methane flux, vertical gradient and mixing ratio measurements in a tropical forest, *Atmos. Chem. Phys.*, *11*, 7943–7953, doi:10.5194/acp-11-7943-2011.

Spivakovsky, C. M., et al. (2000), Three-dimensional climatological distribution of tropospheric OH: Update and evaluation, *J. Geophys. Res.*, *105*(D7), 8931–8980, doi:10.1029/1999JD901006.

van der Werf, G. R., J. T. Randerson, G. J. Collatz, L. Giglio, P. S. Kasibhatla, A. F. Arellano Jr., S. C. Olsen, and E. S. Kasischke (2004), Continential-scale partitioning of fire emissions during the 1997 to 2001 El Niño/La Niña period, *Science*, *303*, 73–76, doi:10.1126/science.1090753.

Wania, R. (2007), Modelling northern peatland land surface processes, vegetation dynamics and methane emissions, PhD thesis, Univ. of Bristol, Bristol, U. K.

Wuebbles, D. J., and K. Hayhoe (2002), Atmospheric methane and global change, *Earth Sci. Rev.*, *57*, 177–210, doi:10.1016/S0012-8252(01)00062-9.

Yokelson, R. J., T. Karl, P. Artaxo, D. R. Blake, T. J. Christian, D. W. T. Griffith, A. Guenther, and W. M. Hao (2007), The Tropical Forest and Fire Emission Experiment: Overview and airborne fire emission factor measurements, *Atmos. Chem. Phys.*, *7*, 5175–5196, doi:10.5194/acp-7-5175-2007.